JOURNAL OF PROPULSION AND POWER
Vol. 20, No. 2, March–April 2004

Simulations of Normal Shock-Wave/Boundary-Layer Interaction Control Using Mesoflaps

R. K. Jaiman,* E. Loth,† and J. C. Dutton‡
University of Illinois at Urbana–Champaign, Urbana, Illinois 61801

Computations were performed to investigate the flowfields of normal shock-wave/boundary-layer interactions with mesoflap control. The passive control (no feedback included) concept involves placing a mesoflap streamwise array beneath the interaction and allowing high-pressure air from the flow downstream of the shock wave to recirculate through a cavity into the low-pressure flow upstream of the wave. The case of a normal shock at a Mach number of 1.4 interacting with the turbulent boundary layer on a flat wall was first considered, and the predictions yielded reasonable comparison with experimental results. A number of fixed-deflection mesoflap simulations were then performed to understand the correlations between flap deflections, downstream boundary-layer characteristics, and stagnation pressure recovery. The prescribed steady-state deflections were based on qualitative aeroelastic experimental observations. It was found that the magnitude of the deflection of the upstream mesoflaps is key to providing a significantly increased "lambda-foot" benefit, which is critical for improved stagnation pressure recovery. The number of flaps and their locations were also found to affect the stagnation pressure recovery and downstream boundary-layer characteristics significantly. However, it was found that cavity depth does not play a significant role in stagnation pressure recovery.

Introduction

NORMAL shock-wave/boundary-layer interaction (SBLI) is a frequently occurring phenomenon that must be considered in supersonic inlet design. In supersonic inlets, deceleration of the flow is achieved through a succession of oblique shock waves followed by a terminal normal shock. Boundary layers form on the inlet surfaces and interact with the shock system, giving rise to various SBLIs. The inlet is carefully designed to minimize stagnation pressure losses during the compression process. Each interaction of oblique/normal shock waves with the boundary layer causes stagnation pressure losses, hence, reducing engine efficiency. Thus, successfully controlling SBLIs has the potential to improve supersonic inlet performance greatly. Furthermore, problems arise if shock-induced separation occurs because the accompanying unsteadiness can lead to engine unstart, which requires that the entire propulsion system undergo a restart sequence during flight. The conventional method of solving this problem is to use boundary-layer bleed. However, this can lead to substantial bleed drag penalities.[1]

A number of techniques have been developed to control the detrimental effects of a shock wave impinging on a boundary layer. Previous research efforts[2–4] on transonic airfoils with shock/boundary-layer interaction control have investigated recirculating flow-control techniques by employing natural recirculation in a cavity beneath the interaction region through slots or holes. These techniques are often effective in eliminating flow separation and reducing wave and viscous drag. However, the performance of conventional recirculation techniques can deteriorate at off-design conditions, and these methods can induce a negative impact on boundary-layer characteristics, resulting in a substantial increase in viscous drag.[3,4] Recently, flow control using recirculation that is, passive control with no feedback, has been suggested as a promising method to reduce the detrimental effects of strong shock waves, specifically for supersonic inlets.

In the mesoflaps for aeroelastic recirculating transpiration (MART) system,[5–9] an array of small flaps is placed beneath the shock foot (Fig. 1). These flaps are fixed at their upstream end to a spar, whereas the majority of the flap can deflect aeroelastically according to the pressure loads imposed by the shock system, resulting in flow recirculation in the cavity similar to that for conventional holes or slots. The flaps downstream of the shock foot deflect downward in response to the pressure increase across the shock. This allows for removal of the low-momentum portion of the boundary layer in a fashion similar to conventional boundary-layer bleed. Upstream of the shock, however, the flaps deflect upward into the low-pressure region preceding the shock system. The flow bled off through the downstream flaps is reinjected through the upstream flaps, thus, energizing the low-momentum portion of the upstream boundary layer. Because the flap deflections are kept relatively small (generally a fraction of the incoming boundary-layer displacement thickness), the MART system possesses an aerodynamic advantage over conventional recirculation control using holes or slots by allowing for nearly tangential bleed downstream and nearly tangential injection upstream. Furthermore, the flaps revert to a nearly smooth solid surface for subsonic freestream conditions, thereby minimizing the roughness and increase in friction drag associated with conventional recirculation-control techniques at off-design (subsonic) conditions. Note that this recirculation control is passive, in the sense that it does not include any feedback and does not remove or add any net mass flow.

Previous experimental work[5,6] for both impinging-oblique and normal-shock interactions has shown that a mesoflap control system utilizing aeroelastic flaps can produce both better total pressure recovery and decreased boundary-layer thickness downstream of the interaction under certain conditions. In particular, mesoflap control designs for a normal-shock/boundary-layer interaction were examined experimentally by Hafenrichter et al.[6] for various flap thicknesses, and it was found that there exists an optimum flap thickness and, therefore, flap deflections, such that one of the cases significantly outperformed all other cases in terms of both stagnation pressure recovery and downstream boundary layer characteristics.

Numerical simulation studies have been performed on the impingement of an oblique shock in the middle of various mesoflap arrays.[8] In a recent study, Kim et al.[9] conducted numerical simulations to study the potential capability of mesoflap arrays to control ramp-generated oblique SBLIs. The simulation of a 16-deg

Received 3 February 2003; revision received 2 September 2003; accepted for publication 10 September 2003.

*Graduate Research Assistant, Department of Aerospace Engineering. Student Member AIAA.

†Professor, Department of Aerospace Engineering, 306 Talbot Laboratory, 104 South Wright Street; loth@uiuc.edu. Associate Fellow AIAA.

‡Professor, Department of Mechanical and Industrial Engineering. Associate Fellow AIAA.

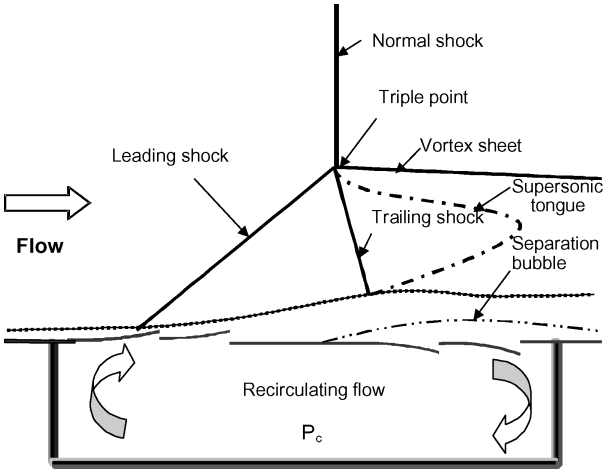

Fig. 1a Basic flow features for mesoflap control of SBLI.

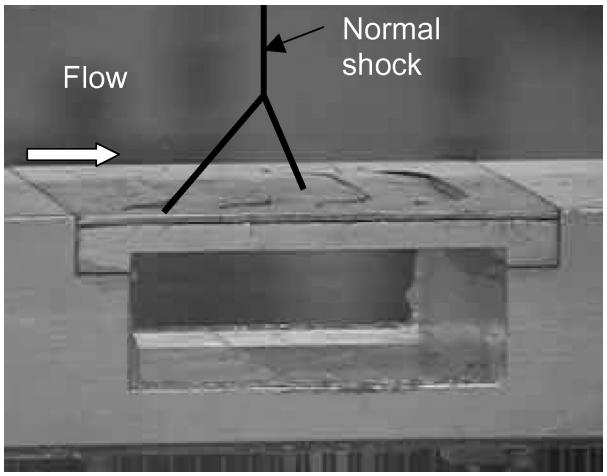

Fig. 1b Upstream and downstream flap deflections during an experiment.

compression corner in $M = 2.85$ flow showed significant improvement in total pressure recovery for the mesoflap cases as compared to the solid-wall case. However, there have been no computational investigations of normal-shock interactions (which are critical for both transonic airfoils and supersonic inlets) for the MART concept, which is the objective of the present study.

The purpose of the present numerical investigation is to understand the nature of the flowfield and the effectiveness of mesoflap blowing and bleeding in controlling normal SBLIs that are similar to the terminal normal-shock interaction in a supersonic inlet. In addition, the current computational findings and predictions are compared with experimental results whenever possible.

Computational Details

Numerical Methods

The computational results were produced using a two-dimensional version of the RAMPANT 4.2 flow solver. The two-dimensional coupled solver is based on a cell-centered finite volume formulation of the Reynolds-averaged Navier–Stokes equations. All convective (inviscid) terms are approximated by the flux-difference splitting scheme of Roe[10] (an upwind-biased flux calculator). The method has shock-capturing capability through the use of a limited reconstruction scheme. Higher-order accuracy is achieved through the use of a piecewise linear interpolation method that follows the principle of the MUSCL procedure.[11] The temporal integration is carried out via a five-step variant of the explicit Runge–Kutta method. The turbulence model can significantly impact the solution, particularly in separated flows; therefore, an assessment of several models for this particular flowfield was undertaken. Two eddy viscosity-based turbulence models were considered for the baseline validation: the Spalart–Allmaras[12] (S–A) one-equation model and the k–ε two-layer two-equation model.[13]

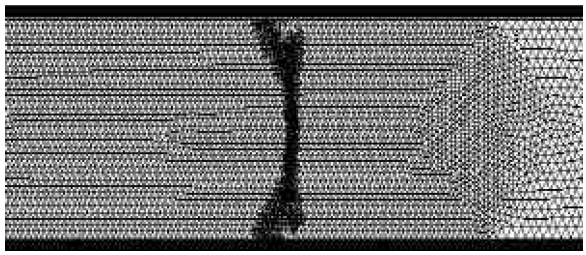

Fig. 2a Hybrid and nonuniform grid system with grid adaptation for solid-wall case.

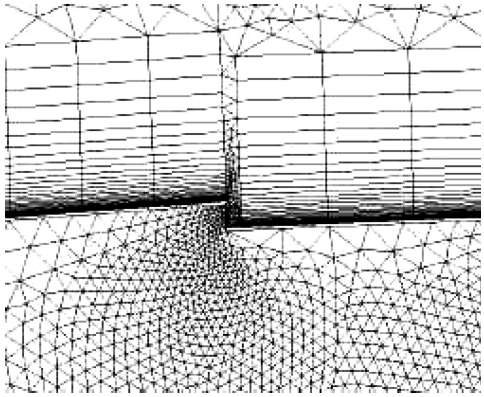

Fig. 2b Enlarged view of grid system near injection flap.

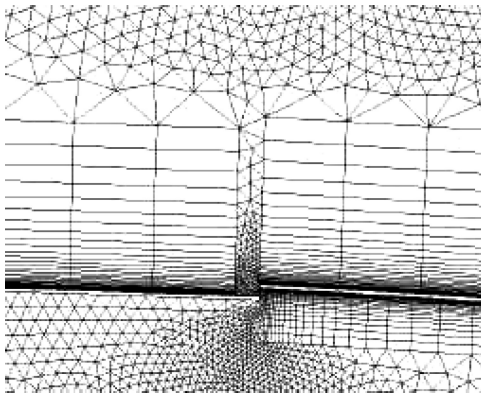

Fig. 2c Enlarged view of grid system near bleeding flap for a mesoflap case.

Mesh Selection

The grid system (Fig. 2a) is composed of a structured boundary-layer mesh in the near-wall region and an unstructured mesh in the outer region and in the vicinity of the flap tips. Figures 2b and 2c show enlarged views of the hybrid grid systems in the regions about the blowing and bleeding flaps of a representative mesoflap case. The structured viscous mesh employed a first gridpoint placement from the wall at y^+ less than unity. A stretching function was used to cluster gridpoints near the wall. Once the wall normal distance exceeded twice the boundary-layer thickness, unstructured grids were constructed, and the unstructured grid zones were also adapted based on density gradients.

Solution Procedure

The boundary conditions on the solid walls were those of an adiabatic wall with no slip. For the supersonic inflow, the flow Mach number, total pressure, and total temperature were specified; the boundary condition at outflow simply fixed the value of the static

pressure. Based on the experiments, the total pressure upstream and the backpressure downstream were applied on the corresponding inflow/outflow boundaries. All simulations were completed by initialization of the domain interior with the flow conditions upstream and downstream of the desired shock location based on shock-jump (Rankine–Hugoniot) relations. This enabled better convergence and also ease in handling the sensitivity of the computations to the backpressure value. To initialize the flowfield in this manner, the grid was generated in parts: one ahead of the shock and one behind the shock. This could be done by declaring the two regions as two different continua, both being the same fluid, but having different pressure and velocity values.

Two methods of convergence acceleration were employed: local time stepping and residual smoothing. Local time stepping involves taking the maximum possible time step, based on the Courant–Friedrichs–Lewy stability criterion, at each grid point separately. Residual smoothing involves increasing the stability limit by implicitly averaging the residuals. All calculations were typically run until the mass and energy residuals reached 10^{-4} (four decades) decay, with shock movement of up to two–three times the incoming boundary-layer thickness over this time frame being deemed acceptable.

Specification of Flap Deflection Distribution

Experimental work[5–7] has shown that flap deflections are far in excess of any fluctuations, such that a steady geometry assumption was reasonable. To avoid the computationally intensive approach of employing fully aeroelastic simulations and to better understand the direct relationship between flap deflection and aerodynamic performance, fixed deflection distributions were employed in the present simulations. These a priori distributions were chosen based on experimental observations, numerical aeroelastic simulations, and theoretical deflections. The use of preset deflections also has the advantage of enabling investigation of the aerodynamic sensitivity to independent changes in upstream or downstream deflections (equivalent to adjusting the flap thickness or stiffness to achieve a desire deflection for a given pressure difference). Figure 1b shows a view of aeroelastically deflected upstream and downstream flaps during an experiment. This photograph was taken in the University of Illinois at Urbana–Champaign (UIUC) tunnel experiments for a four-flap MART case. The shock is located at approximately the middle of the cavity, as shown in Fig. 1b. There are two upward-deflected flaps and two downward-deflected flaps. Note in the Fig. 1b photograph that the most upstream and most downstream flaps are deflected significantly more than the two flaps nearest the shock. This is consistent with the measurements of Gefroh et al.,[5] which showed a gradual increase in static pressure on the surface of the interaction and an approximately constant pressure within the cavity. This pressure distribution is also consistent with steady aeroelastic simulations by Wood et al.[8] Flap geometry and thickness for the current simulations were also specified to be consistent to those used in the experiments conducted in the UIUC tunnel.

In this computational study, two independent deflections were specified, the maximum upward deflection of the first injection flap, $D1$, and the maximum downward deflection of the last bleeding flap, $D2$. The deflections $D1$ and $D2$ are nondimensionalized by the incoming boundary-layer displacement thickness δ_0^*. In the case of four-flaps arrays, the second upstream flap and first downstream flap deflections are taken as one-half of the first injection flap deflection, $\frac{1}{2}D1$, and one-half of the second bleeding flap deflection, $\frac{1}{2}D2$, respectively. This assumption is based on linear interpolation between the tip deflections of the most upstream and most downstream flaps and is qualitatively consistent with the experimental aeroelastic deflections and pressure distributions.[8] This admittedly empirical method of prescribing flap deflections was used to obtain a wide range of parametric and sensitivity studies of mesoflap effects on aerodynamic performance.

In the case of six-flap arrays, the interpolation just described can be extended such that one extra upstream flap is inserted with deflection $\frac{3}{4}D1$, between the most upstream and near-shock upstream flaps. Similarly, a downstream flap is inserted with deflection $\frac{3}{4}D2$, between the most downstream and near-shock downstream flaps.

Parameters of Interest

To obtain a quantitative measure of how the mesoflap deflections and other related parameters affect overall stagnation pressure recovery, it was decided to integrate the computed total pressure profiles to evaluate the mass-averaged total pressure $\bar{P}_t$ for each of the cases, where

$$\bar{P}_t = \frac{\int_{y=0}^{h} \rho u P_t \, \mathrm{d}y}{\int_{y=0}^{h} \rho u \, \mathrm{d}y} \tag{1}$$

and where h is the channel height. Furthermore, the mass-averaged total pressure recovery is nondimensionalized by the inlet stagnation pressure P_0 to give the total pressure recovery parameter α,

$$\alpha = \bar{P}_t / P_0 \tag{2}$$

This parameter is useful because it is proportional to the overall stagnation pressure recovery. Another useful derived performance parameter can be defined as

$$\beta = (\alpha - \alpha_{\mathrm{sw}})/(1 - \alpha_{\mathrm{sw}}) \tag{3}$$

where α is the total pressure recovery parameter for any controlled case and α_{sw} is the total pressure recovery parameter for the uncontrolled solid-wall case. For the inviscid isentropic case, the value of β will be unity. For the viscous and/or nonisentropic case, there will be a total pressure loss such that β will be less than unity. The parameter β can also take on negative values when the total pressure recovery is poorer than for the solid-wall reference case. From its definition, it can be seen that the parameter β gives the fraction of possible total pressure recovery improvement that is obtained (between the solid-wall case and ideal isentropic compression) for a given case with mesoflap control. Clearly, β does not provide actual improvement in total pressure recovery across a shock; however, it gives a relative and scaled total pressure recovery improvement to that possible. In addition, integral boundary-layer parameters such as the incompressible displacement thickness δ^*, incompressible momentum thickness θ, and shape factor H, δ^*/θ, were investigated.

Results and Discussion

Solid-Wall Validation

This study is used for validation of the solid-wall/shock-interaction numerical results and as a reference case for comparison of the performance of the mesoflap control system. The case studied here is that of supersonic flow through a constant cross-section duct. In this case, the backpressure at the exit of the tunnel is sufficiently high to cause a strong normal shock within the constant cross-section region (Fig. 2). The calculation was performed for an inlet Mach number of 1.4. This Mach number is consistent with that of previous measurements and is also in the range of Mach 1.3–1.5 suggested by Boeing and NASA engineers as typical of a terminating normal shock in a supersonic inlet. The incoming boundary-layer thickness, which was 2.6 mm in both the experiments[6] and current computations, was also used as the reference length for the results presented herein.

A normal shock with a lambda foot can be seen in the computed Mach number contours (Fig. 3b), which are comparable to the experimental shadowgraph (Fig. 3a). The lambda foot exhibits the expected short leading oblique shock wave with a small triangular region of still supersonic flow downstream, terminated by a nearly normal trailing shock. The numerical bifurcation point height is in good agreement with the experimental result (approximately three boundary-layer thicknesses above the wall). The boundary layer downstream of the interaction is clearly significantly thicker than the incoming boundary layer.

In Figs. 4a and 4b, the incoming and outgoing velocity profiles, predicted with the S–A and k–ε two-layer models, are

compared with the experimental data[6] at the upstream location, $x^* = -17.3$, and the downstream location, $x^* = 19.3$, respectively. Herein, streamwise location, $x^* = (x - x_0)/\delta_0$, is nondimensionalized by the incoming boundary-layer thickness δ_0 and is defined to be zero at the shock position x_0. The incoming velocity profile for both models agrees well with the experimental data. The outgoing velocity profiles are found to have some discrepancies with the experimental profiles.[6] One can see from Fig. 4 that both turbulence models overpredict the velocity profiles near the wall, which implies that they develop too fast after the shock interaction as compared to the experimental data. Farther from the wall, the k–ε model prediction generally agrees better with the experimental outgoing velocity profile than does the S–A model prediction.

Figure 4c shows the skin-friction distributions for both models and the experimental data at four downstream locations.[7] There is good agreement for both predictions, but especially for the S–A model. Figure 4d shows the surface static pressure distribution (normalized by the inlet stagnation pressure P_0) for the solid-wall reference case. The static pressure distributions of the S–A and k–ε two-layer models compare reasonably well with the experimental data. However, the k–ε two-layer model gives a slightly better prediction.

In review, experiments and computations for both the S–A and k–ε two-layer models generally agree on a number of fundamental features at various stages of the flow development. However, the k–ε two-layer model was chosen for the bulk of the study because it gave somewhat better predictions of the centerline wall pressure (Fig. 4d) and outgoing mean velocity profiles (Fig. 4b). In addition, the k–ε two-layer model was found to be more robust with respect to convergence for the fixed-deflection mesoflap cases, which have complex hybrid unstructured grids.

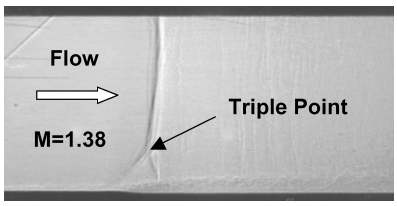

a) Shadowgraph

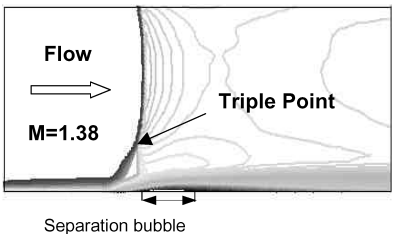

b) Mach number contours

Fig. 3 Comparison between shadowgraph and Mach number contours for solid-wall case.

Effects of Mesoflap Deflections

Several four-flap fixed-deflection mesoflap simulations (28 cases of different upstream and downstream flap deflections) have been performed to understand the correlations between flap deflections and subsequent boundary-layer characteristics and stagnation pressure recovery. The physical scale of the deflections is lower bounded by the limitation that they should be large enough to ensure sufficient mass bleed of the boundary layer and to take advantage of the high convection speeds within the sonic region to drive transpiration. The

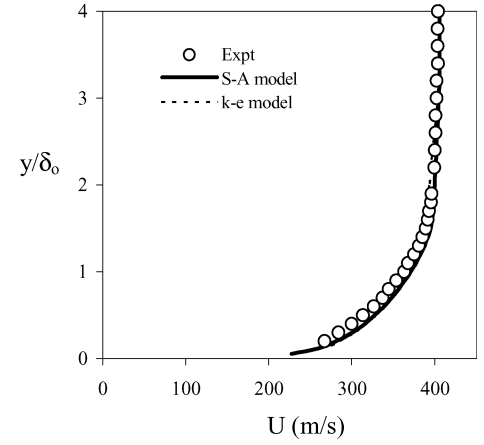

a) Incoming velocity profiles at $x^* = -17.3$

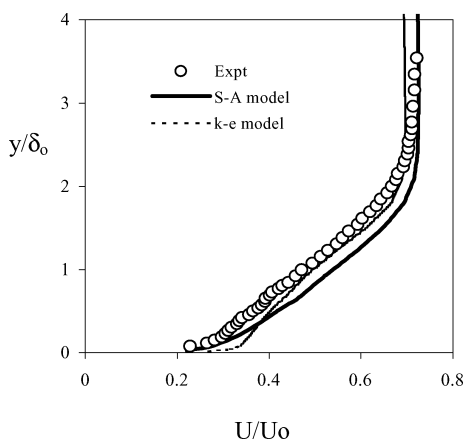

b) Outgoing velocity profiles at $x^* = 19.3$

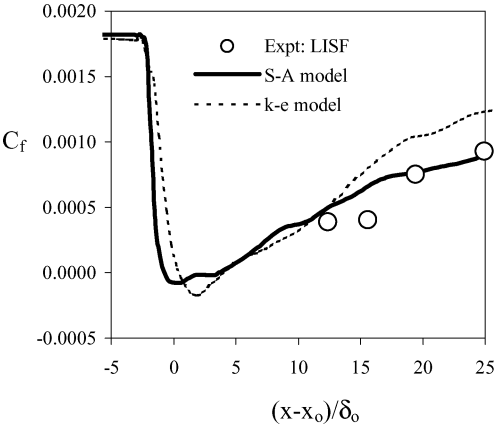

c) Comparison of streamwise variation of skin friction

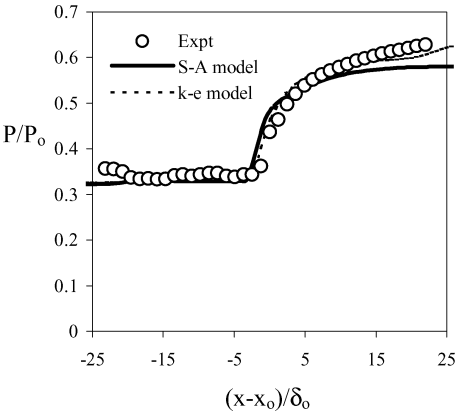

d) Comparison of streamwise variation of surface static pressure

Fig. 4 Comparison of mean velocity profiles.

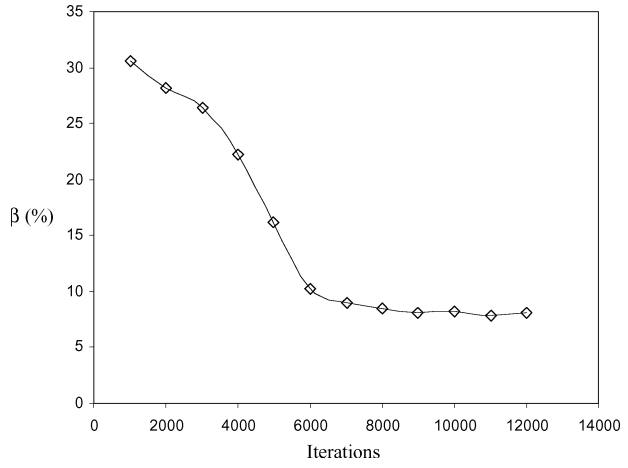

a) Solution convergence

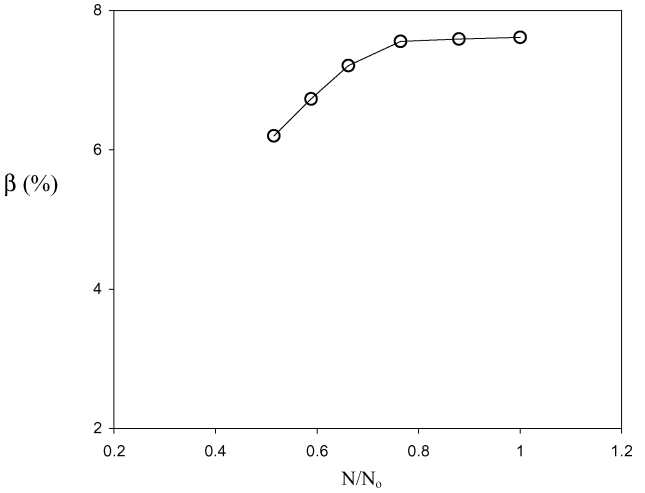

b) Grid-independence study

Fig. 5 Total pressure recovery improvement index (β).

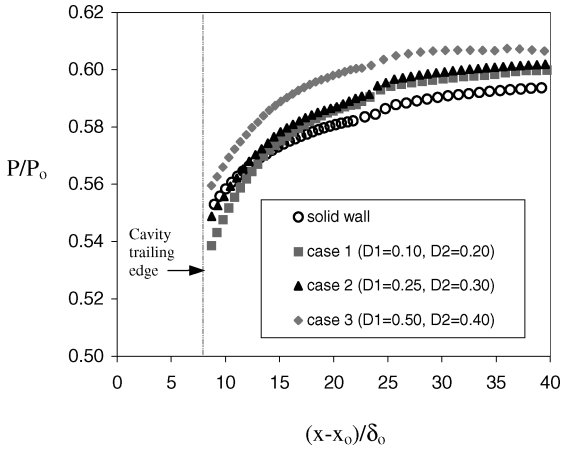

a)

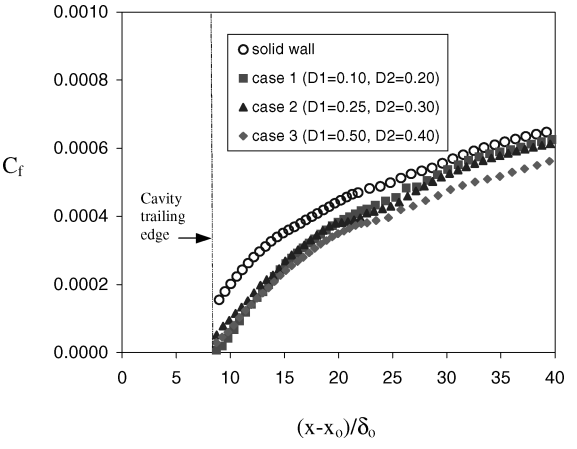

b)

Fig. 6 Streamwise variations of a) surface static pressure and b) skin friction downstream of the interaction.

deflections were upper bounded by the limitation that the deflections themselves did not produce significant additional local separations. Thus, to investigate the effect of deflection magnitudes, the upstream and downstream flap deflections were varied from $0.2\delta_0^*$ to $0.7\delta_0^*$. Before detailed fixed-deflection parametric and sensitivity studies were performed, convergence-check and grid-independence studies were carried out for a sample mesoflap case ($D1 = 0.50$ and $D2 = 0.40$).

Figure 5a shows the convergence history of the total pressure recovery improvement index β for the fixed-deflection mesoflap case. Satisfactory convergence of β can be seen after 8000 iterations. Furthermore, Fig. 5b shows the value of β for various grid densities that is, number of finite volume control cells, where grid density N is normalized by the finest grid resolution N_0. It is apparent that a grid-independent solution has been obtained for the finest grid density N_0.

Figure 6a shows the static pressure distribution downstream of the cavity for three representative fixed-deflection mesoflap cases, as well as the solid-wall reference case. Note that the magnitude of the mesoflap deflections has a significant effect on the surface static pressure distribution downstream of the interactions. The downstream pressure of the lesser-deflected case 1 ($D1 = 0.10$ and $D2 = 0.20$) and case 2 ($D1 = 0.25$ and $D2 = 0.30$) is initially less than for the solid-wall reference case, but eventually rises above that of the solid wall. However, the downstream pressure of the greater-deflected case 3 ($D1 = 0.50$ and $D2 = 0.40$) is significantly higher than for the reference case in the entire downstream region.

In Fig. 6b, the variations of the skin-friction distribution C_f downstream of the shock/boundary-layer interaction for the three representative fixed-deflection mesoflap cases are compared with that for the solid-wall reference case. For all fixed-deflection flap cases, it is found that skin friction increases in the downstream direction. These skin-friction variations show an approximately linear increase in the most downstream region. Immediately downstream of the cavity, the C_f for all mesoflap cases is less than that for the solid wall, indicating that the boundary layer is more prone to separation with mesoflap control. However, farther downstream, C_f for the lesser-deflected cases approaches that for the solid wall.

Figures 7a–7d show numerical Mach number contours Figs. 7a and 7b and experimental shadowgraphs Figs. 7c and 7d for normal SBLIs with mesoflap control. The effects of the control are immediately apparent in both the experimental shadowgraphs and the Mach number contours when compared to the small lambda structure of the solid-wall case (Figs. 3a and 3b). However, no direct quantitative comparisons between the computations and experiments can be made because the computations were based on ad hoc flap deflection assumptions, whereas experimental flap deflections are achieved by the nonlinear aeroelastic response of a nickel–titanium alloy termed nitinol (a shape memory alloy). The mesoflap case exhibits a leading, oblique shock wave originating from the start of the first injection flap, followed farther downstream by additional oblique shock waves and, thus, a significantly smeared shock-foot structure. The strength of the oblique waves is also seen to increase with increasing deflection of the flaps and, hence, with the strength of blowing (in both the simulations and experiments). The predicted Mach number contours indicate a very low-speed recirculation within the cavity, accompanied by tangential injection upstream of the shock and bleed downstream.

Figure 8a shows normalized total pressure profiles, $P_t/P_{0,}$ at location $x^* = 23.0$. The profiles for the mesoflap control cases

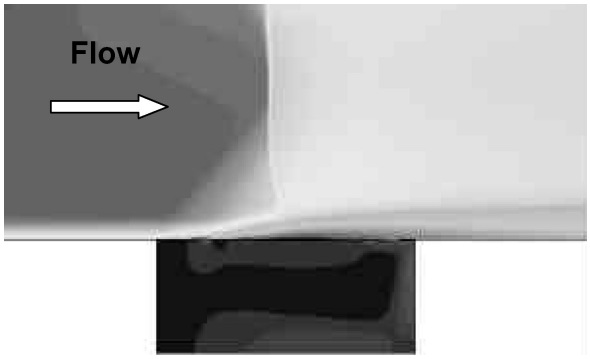

a)

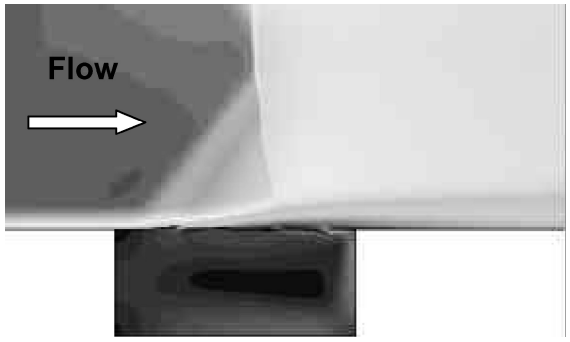

b)

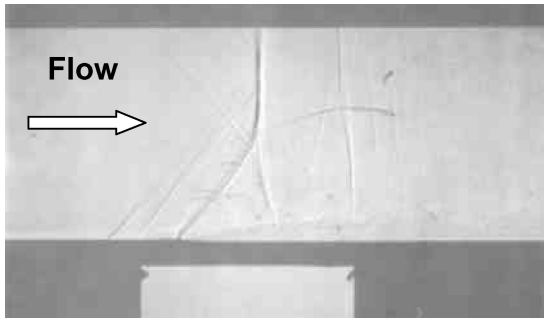

c)

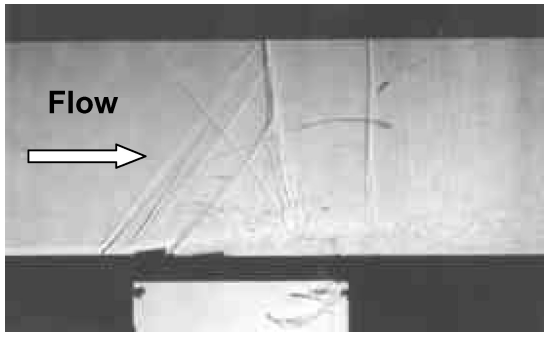

d)

Fig. 7 Mach number contours for fixed-deflection four-flap cases: a) $D1 = 0.25$ and $D2 = 0.3$ (lesser deflection flap case), b) $D1 = 0.5$ and $D2 = 0.4$ (greater deflection flap case), c) shadowgraphs for aeroelastic thicker four-flap cases,[6] and d) for the thinner four-flap case.

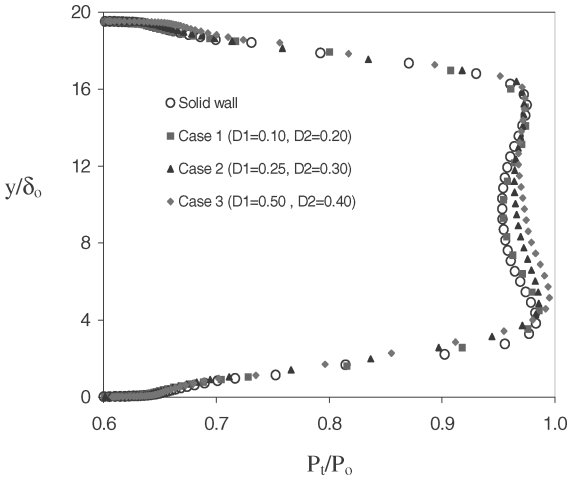

a) Stagnation pressure profiles

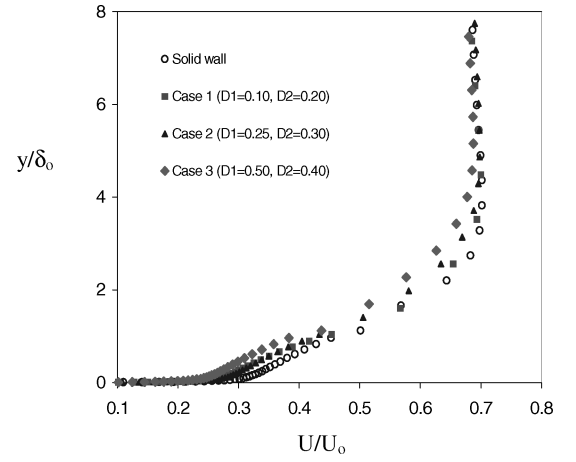

b) Normalized mean velocity profiles

Fig. 8 Comparison of various fixed-deflection four-flap cases at $x^* = 23.0$.

show significant improvement over the solid wall. Furthermore, it is also quite apparent that cases with larger deflected upstream flaps, that is, greater extent of the lambda foot, give higher total pressure recovery. Figure 8b depicts mean velocity profiles for the same fixed-deflection cases and the solid wall at the same streamwise location, $x^* = 23.0$. The velocity profiles of the fixed-deflection cases indicate that the mesoflaps reduce the fullness of the boundary layer, especially for the greater-deflected case. This is an expected tradeoff between the total pressure recovery and boundary-layer displacement thickness and is also observed in the experiments.

In Figs. 9a and 9b, the normalized mass-averaged total pressure α and displacement thickness are shown for the solid-wall case and three sample fixed-deflection mesoflap cases at various streamwise locations. Because of viscous losses, the total pressure recovery decreases with increasing streamwise distance. All fixed-deflection mesoflap cases predict higher total pressure recovery compared with the solid-wall case at any particular streamwise location, with the increase correlated with larger deflections. In addition, the total pressure recovery improvement index percent of β is shown for two limiting values, $\beta = 0$ and 10%, in Fig. 9a. In general, β is approximately independent of downstream measurement location for each configuration, which makes it a convenient measure of the flow control effect. In all of the flap cases, the displacement thickness (Fig. 9b) increases with increasing streamwise distance downstream of the SBLI. Note that the displacement thickness also increases as the deflection of the upstream flaps increases. The displacement thickness of all mesoflap cases is larger than for the solid-wall case, indicating that the flow control does not generally reduce boundary-layer thickness under these conditions.

Figure 10a shows the total pressure recovery improvement index (percent β) contours for various fixed-deflection cases of different combinations of the most upstream flap deflection $D1$ and the most downstream flap deflection $D2$. This study is done to find approximate optimal deflections in terms of total pressure recovery. In general, the optimum deflections were found to be of the order of one-half of the displacement thickness of the incoming boundary

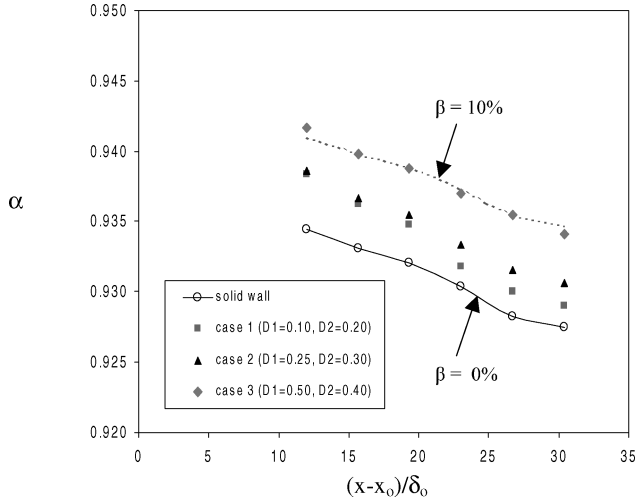

a) Mass-averaged total pressure

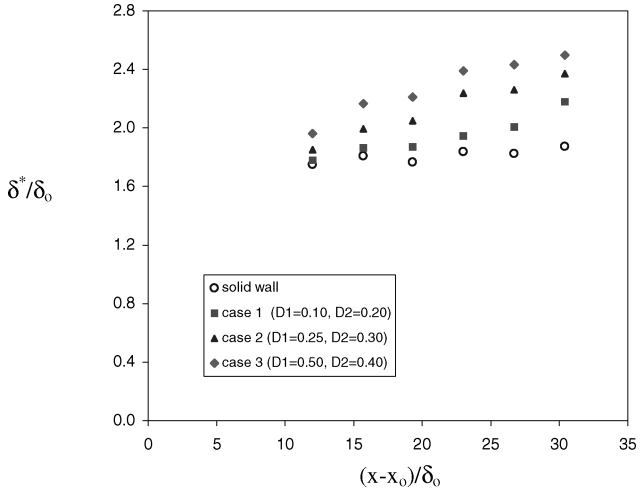

b) Incompressible displacement thickness

Fig. 9 Streamwise variations of normalized.

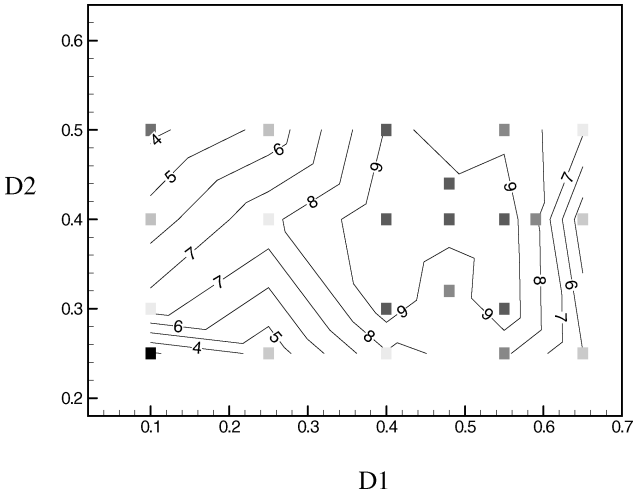

a) Percentage total pressure recovery improvement index (β) contours

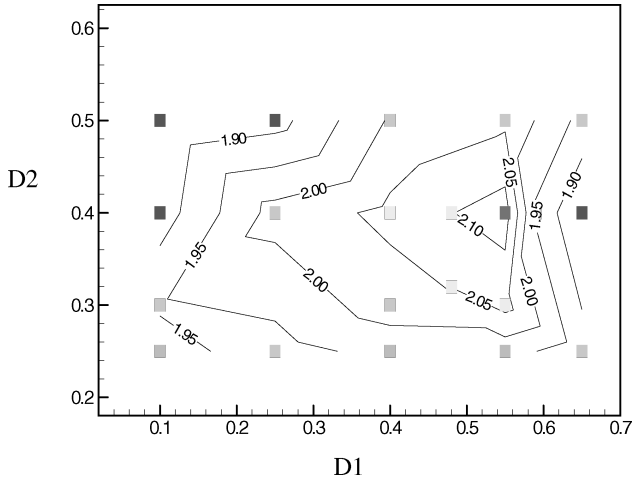

b) Incompressible shape factor *H* contours

Fig. 10 Fixed deflection results for various flap deflections at $x^* = 23.0$.

layer. The upstream deflection of the mesoflaps is a key to providing a significantly increased lambda-foot benefit, and the optimum upstream deflections should be somewhat larger than the optimum downstream deflections, that is, $D1 > D2$. The smaller downstream flap deflections are attributed to the importance of bleeding only a modest amount of the boundary layer (critical for boundary-layer recovery), whereas the comparatively larger upstream deflections are important to provide an oblique precompression of the supersonic upstream flow.

Figure 10b depicts the incompressible shape factor for various fixed-deflection cases at $x^* = 23.0$. The contour lines follow a somewhat different trend compared with the pressure recovery contours in Fig. 10a. Nevertheless, the incompressible shape factor is found to be highest near the region of optimal flap deflections for total pressure recovery. This indicates that the mean velocity profiles become less full and the boundary layers are thicker for the cases of higher total pressure recovery.

Effect of Number of Mesoflaps

Figure 11a shows the pressure recovery improvement index for fixed-deflection cases that have varying but equal numbers of upstream N_{up} and downstream N_{down} flaps that is, $N_{\text{up}} = N_{\text{down}}$, and by fixing the number of downstream flaps at two that is, $N_{\text{down}} = 2$, where flap length is fixed. Figure 11 indicates a monotonically increasing value of pressure recovery as the overall flap number increases, but with a saturation effect near $N_{\text{flaps}} = 6$–7. The saturation may be related to the shock bifurcation point having reached the upper boundary layer. A monotonically increasing trend of incompressible displacement thickness with number of flaps can be seen in Fig. 11b. The increase in total pressure is attributed to the larger lambda foot caused by a larger number of upstream flaps, whereas the decrease in boundary-layer fullness is attributed to the roughening caused by the additional flaps.[14] In general, the pressure recovery improvement index β seems to be only a function of N_{flaps}, whereas the boundary-layer displacement thickness δ^* tends to be somewhat smaller for symmetric flap numbers, that is, $N_{\text{up}} = N_{\text{down}}$. The increase in boundary-layer displacement thickness is generally undesirable because it relates to a significant thickening of the boundary layer. However, the increases are modest (approximately 10% over the solid-wall condition), and if boundary-layer aspects are important, then smaller numbers of flaps may be appropriate. For example $N_{\text{flaps}} = 2$ or 4 tends to yield a significant increase in β with only a minor increase in δ^*.

Effect of Cavity Depth

Figure 12a shows the effect of cavity depth on β for six values of the depth for a four-flap mesoflap system. The simulations show that an increase in cavity depth somewhat reduces the pressure gradients in the interaction region and slightly increases the mass-weighted total pressure recovery improvement at the downstream locations. However, the overall total pressure recovery is not appreciably affected by cavity depth for depths larger than about one incoming boundary-layer thickness, as seen in Fig. 12a. It is, therefore, evident that cavity depth does not play a significant role in precompression or smearing of the normal shock. This is also consistent with

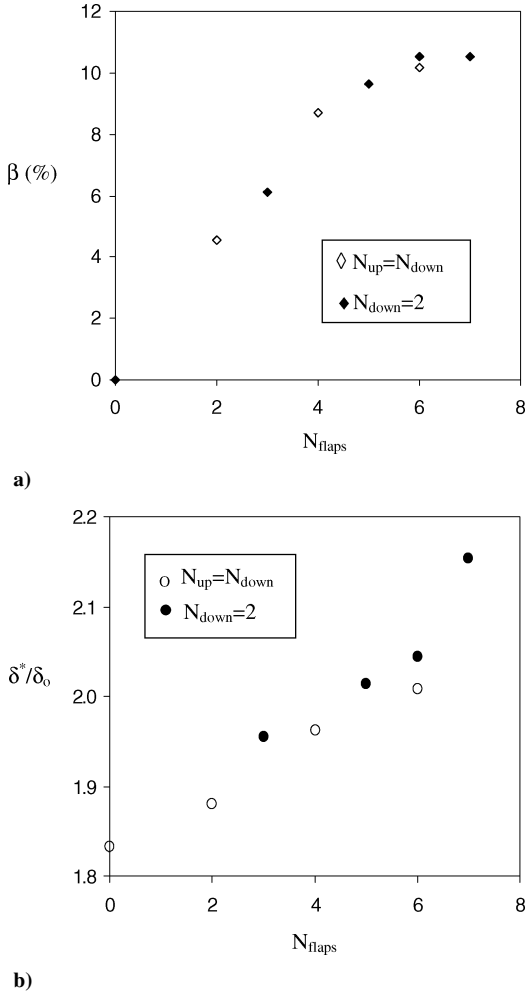

Fig. 11 Total number of flaps effect at $x^* = 23.0$ on a) total pressure recovery improvement index and b) normalized displacement thickness.

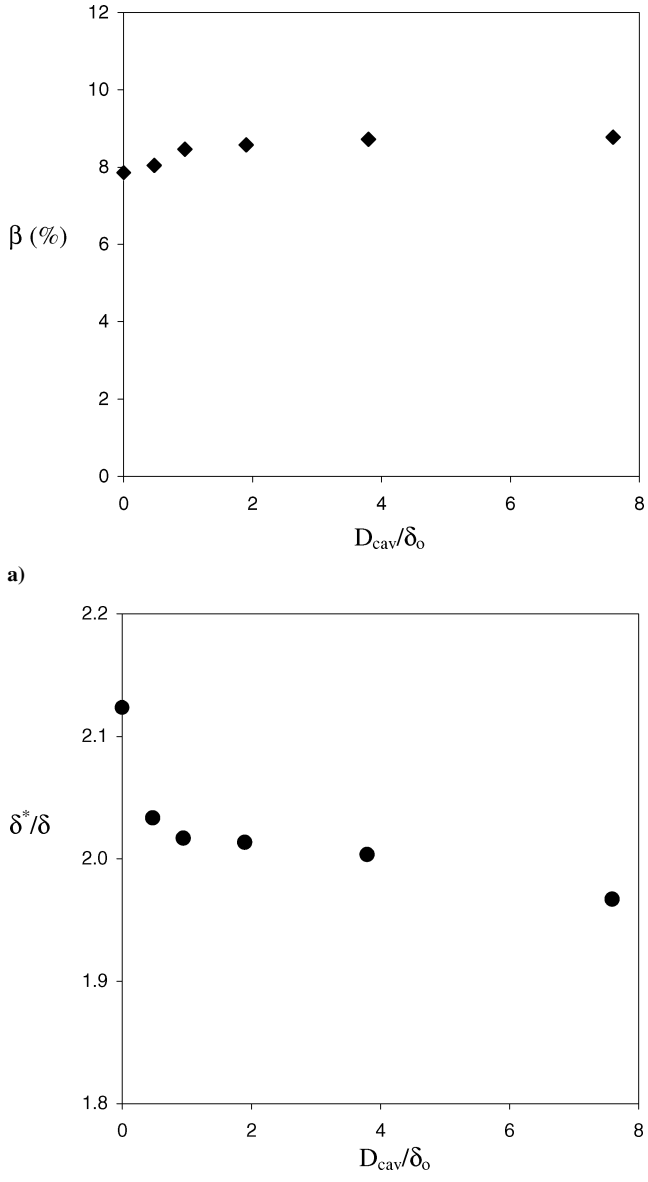

Fig. 12 Effect of cavity depth at $x^* = 23.0$ on a) total pressure recovery improvement index and b) normalized incompressible displacement thickness.

previous studies.[3–4] In terms of the effects of the various recirculating flow control parameters, Bur et al.[4] found that cavity depth had no significant effect on the external flow for a porous-plate-covered cavity system. The no-cavity that is, no-recirculation, $D_{cav}/\delta_0 = 0.0$, case also shows a significant amount of total pressure recovery improvement. This suggests that the majority of the mesoflap benefit stems from the protrusion of the upstream flaps into the supersonic freestream flow (and not necessarily from the mass injection or ramp angle).

Figure 12b shows the effect on the displacement thickness for various values of the cavity depth. Note that the no-recirculation that is, no-cavity, case shows a significant rise in the displacement thickness as compared to the other cavity depth cases. This suggests that the cavity recirculation for the mesoflap cases is primarily important for boundary-layer rehabilitation. Similar to the total pressure recovery, the displacement thickness is also not significantly affected by cavity depth for depths beyond about $1\delta_0$. These findings about the cavity-depth effect on the flow-control performance seem important and attractive for aircraft applications because the cavity can be made quite shallow and, therefore, will take up little space.

Apart from the aforementioned effects, flap position and flap length have been also found to affect stagnation pressure recovery and boundary layer characteristics significantly. (Consult Refs. 14 and 15 for details.) Further tuning of upstream flap positions or length can lead to significant improvement in the total pressure recovery. Nevertheless, the original flap locations and length used herein were found to be already approximately optimized in the consideration of both pressure recovery and boundary-layer characteristics.

Conclusions

Numerical simulations were conducted to study the effects of mesoflaps to control normal-shock/boundary-layer interactions that are typical of supersonic inlet applications. The numerical solutions for the solid-wall case were first compared to experiments, and showed good agreement. For the mesoflap cases, it was observed that the onset of the upstream flap deflections leads to the formation of a series of oblique shock waves, originating from the most upstream flap. Such oblique shock waves allow deceleration of the supersonic flow to take place with relatively small losses of stagnation pressure and are, thus, favored in the inlet over deceleration through a normal shock wave. Apart from the deflection magnitude, the numbers of flaps and their positions have also been found to affect stagnation pressure recovery and boundary layer characteristics significantly. It is found that stagnation pressure recovery rises monotonically with the number of flaps, but typically with a corresponding deterioration in boundary-layer behavior. However, the overall total pressure recovery is not appreciably affected by cavity depth for depths larger than about one incoming boundary-layer thickness. These effects suggest the potential of the mesoflap control system to impact supersonic inlet design positively, for which total pressure recovery is a prime concern.

Acknowledgments

This work was supported under contract F49620-98-1-0490 by Defense Advanced Research Projects Agency with R. Wlezien as Technical Monitor, and the U.S. Air Force Office of Scientific Research, with T. Beutner as Technical Monitor. The authors would also like to thank D. Davis (NASA John H. Glenn Research Center at Lewis Field) and J. Mace (Boeing Phantom Works) for their comments.

References

[1]Gridley, M. C., and Walker, S. H., "Advanced Aero-Engine Concepts and Controls," 86th Symposium, Conf. Proc. 572, AGARD, 1996.

[2]Nagamatsu, H. T., Mitty, T. J., and Nyberg, G. A., "Passive Shock Wave/Boundary-Layer Control of a Helicopter Rotor Airfoil in a Contoured Transonic Wind Tunnel," AIAA Paper 87-0438, Jan. 1987.

[3]Raghunathan, S., and Mabey, D., "Passive Shock-Wave/Boundary-Layer Control on a Wall-Mounted Model," *AIAA Journal*, Vol. 25, No. 2, 1987, pp. 275–278.

[4]Bur, R., Delery, J., Corbel, B., Soulevant, D., and Soares, R., "A Basic Experimental Investigation of Passive Control Applied to a Transonic Interaction," *Aerospace Science Technology*, Vol. 1, 1998, pp. 61–73.

[5]Gefroh, D., Loth, E., Dutton, C., and McIlwain, S., "Control of an Oblique Shock/Boundary-Layer Interaction with Aeroelastic Mesoflaps," *AIAA Journal*, Vol. 40, No. 12, 2002, pp. 2456–2466.

[6]Hafenrichter, E. S., Lee, Y., Dutton, C., and Loth, E., "Experiments on Normal Shock/Boundary Layer Interaction Control Using Aeroelastic Mesoflaps," *Journal of Propulsion and Power*, Vol. 19, No. 3, 2003, pp. 464–472.

[7]Lee, Y., Hafenrichter, E. S., Jaiman, R. K., Orphanides, M. J., Dutton, J. C., and Loth, E., "Skin Friction Measurements in Normal Shock Wave/Turbulent Boundary-Layer Interaction Control with Aeroelastic Mesoflaps," AIAA Paper 2002-0979, Jan. 2002.

[8]Wood, B., Loth, E., and Geubelle, P., "Simulations of Aeroelastic Mesoflaps for Shock/Boundary-layer Interaction," *Journal of Fluids and Structures*, Vol. 16, No. 8, 2002, pp. 1127–1144.

[9]Kim, S. D., Loth, E., and Dutton, J. C., "Simulations of Mesoflap Flow Control for Ramp Oblique Shock/Boundary-Layer Interactions," AIAA Paper 2002-3117, June 2002.

[10]Roe, P. L., "Approximate Riemann Solvers, Parameter Vector and Difference Schemes," *Journal of Computational Physics*, Vol. 43, 1981, pp. 357–372.

[11]van Leer, B., "Towards the Ulimate Conservative Difference Scheme. IV. A New Approach to Numerical Convection," *Journal of Computational Physics,* Vol. 23, 1977, pp. 276–299.

[12]Spalart, P. R., and Allmaras, S. R., "A One-Equation Turbulence Model for Aerodynamic Flows," AIAA Paper 92-0439, Jan. 1992.

[13]Launder, B. E., and Shima, N., "Second-Moment Closure for the Near-Wall Sublayer: Development and Application," *AIAA Journal*, Vol. 27, No. 10, 1989, pp. 1319–1325.

[14]Jaiman, R. K., Loth, E., and Dutton, J. C., "Numerical Simulations of Normal Shock-Wave/Boundary-Layer Interaction Control Using Mesoflaps," AIAA Paper 2003-0445, Jan. 2003.

[15]Jaiman, R. K., "Simulations of Normal Shock-Wave/Boundary-Layer Interaction Control Using Mesoflaps," M.S. Thesis, Dept. of Aeronautical and Astronautical Engineering, Univ. of Illinois at Urbana–Champaign, Urbana, IL, Dec. 2002.